JOURNAL OF NEUROPHYSIOLOGY
Vol. 71, No. 2, February 1994. *Printed in U.S.A.*

A Simulation of Action Potentials in Synaptic Boutons During Presynaptic Inhibition

BRUCE GRAHAM AND STEPHEN REDMAN
Centre for Information Science Research and Division of Neuroscience, The John Curtin School of Medical Research, The Australian National University, Canberra, A.C.T., 2601, Australia

SUMMARY AND CONCLUSIONS

1. During presynaptic inhibition, an increased conductance in the membrane of the presynaptic bouton is presumed to reduce the action potential, thereby reducing transmitter release. The object of the simulation has been to determine the magnitude of a chloride conductance required to reduce transmitter release, for various diameters of synaptic boutons, connected to axons with diameters in the range 0.1–1.0 μm.

2. A propagating action potential was simulated in axons connected to either side of a hemispherical bouton. The axons could be myelinated or unmyelinated, while the bouton membrane could be passive, a node of the myelinated nerve, or have the same active properties as the attached unmyelinated nerve. Membrane properties of the axons were derived from mammalian data and scaled to 37°C.

3. A steady-state chloride conductance was included in the bouton membrane, with $E_{Cl} = -40$ mV. The amplitude of the action potential in the bouton was calculated for different diameters of axon and bouton and for different magnitudes of chloride conductance.

4. Using published data on the relationship between the amplitude of a presynaptic action potential and the resulting postsynaptic potential, the relationship between the chloride conductance and the postsynaptic response was calculated for different geometries. Transmitter release was reduced when an action potential was 90 mV or smaller, with no transmission for action potentials smaller than 50 mV.

5. Conductance increases in the range 3 to 10 nS were required to reduce the action potential to 90 mV, depending on the diameter of the axon (0.5–1.0 μm), diameter of the bouton (3–6 μm), whether the bouton had passive or active membrane, and whether the axon was myelinated or unmyelinated. A 3 μm passive bouton connected to a 0.5 μm myelinated axon was most sensitive to the effects of a chloride conductance, while a 6 μm active bouton connected to a 1 μm myelinated nerve was least sensitive to the effects of a chloride conductance.

6. The reduction in the action potential was compared when $E_{Cl} = -40$ mV and when $E_{Cl} = E_{rest} = -80$ mV. Inactivation of the sodium conductance by terminal depolarization was the dominant influence on the amplitude of the action potential.

7. Conductances that were sufficient to completely block synaptic transmission at a bouton were insufficient to prevent the spread of the action potential away from that bouton.

8. Schemes involving three boutons en passant, or three boutons terminating an axon, with the boutons linked by small diameter (0.1–1.0 μm) axons of length 10 μm, required conductances in the range 200 pS–3 nS on all three boutons to reduce the action potential to 90 mV.

9. These calculations are integrated with the quantal conductance for γ-aminobutyric acid (GABA), and the convergence of axoaxonic contacts onto presynaptic terminals to determine whether the conductance increases required for presynaptic inhibition are likely to occur. It is suggested that it will be difficult to achieve a sufficiently large chloride conductance to make a significant reduction in transmitter release. However, the depolarization associated with the chloride conductance may have a direct inactivating action on high threshold calcium channels in the terminal membrane, thereby contributing to presynaptic inhibition.

INTRODUCTION

Presynaptic inhibition was first proposed by Frank and Fuortes (1957) to account for the reduction of Group Ia excitatory postsynaptic potentials (EPSPs) in spinal motoneurons by an inhibitory mechanism that could not be detected postsynaptically. Presynaptic inhibition has since been described at synapses formed by different types of neurons in both vertebrates and invertebrates (reviewed in Burke and Rudomin 1977; Martin 1977; Nicoll and Alger 1979; Watson 1992).

In spinal cord, the axo-axonic contacts which mediate presynaptic inhibition are formed on large S-type boutons that measure 1–5 μm along their long axis (Conradi et al. 1983; Fyffe and Light 1984; Maxwell et al. 1990). Smaller P-type boutons are the presynaptic elements of these axo-axonic synapses. The neurotransmitter released from the P-type boutons is believed to be γ-aminobutyric acid (GABA) (Maxwell et al. 1990; reviewed in Nicoll and Alger 1979). Activation of $GABA_A$ receptors increases a chloride conductance, leading to an outward movement of chloride ions and a depolarization of the nerve terminal. When a nerve impulse activates the postsynaptic terminal membrane, the probability that a vesicle of transmitter is released is reduced during presynaptic inhibition (Clements et al. 1987). While the mechanism by which GABA reduces transmitter release is unknown, the most accepted hypothesis is that the amplitude of the action potential in the nerve terminal is reduced by the shunting effect of the chloride conductance. This causes a reduced calcium influx through voltage-activated channels and a reduction in transmitter release.

Segev (1990) has calculated how the amplitude of an action potential at the terminal region of a Hodgkin-Huxley axon was altered by a conductance increase in the terminal axon or at various distances from the termination. The reversal potential associated with the conductance was assumed to be the same as the resting potential. The action potential was reduced in a graded manner when the conductance change was located at, or within approximately 0.3 space constants (λ) from the termination, and conduc-

TABLE 1. *Comparison of mammalian action potential characteristics at 37°C derived from literature and those obtained from the simulations*

Action Potential Characteristic	Unmyelinated Nerve, diam 0.4 to 1.2 μm	Unmyelinated Model		Myelinated Nerve, diam <2 μm	Myelinated Model	
		1 μm	0.5 μm		1 μm	0.5 μm
Time to peak (μs)	200–600	240	240	100–400	140	160
Duration (ms)	1.2–2.6	2.0	2.0	0.5–1.8	1.0	1.0
Amplitude (mV)	100	110	110	110	110	106
Conduction vel. (m/s)	1–2.5	1.1	0.8	4.5–11	5.0	2.5

tance increases were more effective in reducing the action potential when the terminal region of the axon had passive rather than active membrane. When the terminal region of the axon was converted to a series of varicosities connected by a small diameter (0.1–0.5 μm) axon, the effects of a shunt conductance on the action potential were further enhanced. This simulation showed that a conductance of 10 nS was required on a terminating varicosity to reduce an action potential in the varicosity to 20 mV. After examining a variety of geometrical arrangements of en passant and terminating boutons, Segev concluded that the effects of releasing one, or a few quanta of transmitter at axo-axonic synapses would drastically reduce or block an action potential. This conclusion was based on the peak quantal conductance at the axo-axonic synapse being 21 nS, which is appropriate for glycine but not for GABA.

This paper extends Segev's analysis. We have calculated the effect of a chloride conductance, with a depolarizing reversal potential, on the action potential in an en passant bouton located in either a myelinated or unmyelinated axon. The conductances that generate the action potential have been derived from published data on mammalian nerve (Chiu et al. 1979) and scaled to 37°C. In this scheme, the action potential is reduced by the shunt itself, and by the depolarization the chloride conductance causes in the bouton and the axon. It is shown that inactivation of the sodium current by the depolarization in the terminal and nearby axon causes a much larger reduction in the action potential than the shunt alone. Relationships between action potential amplitude and transmitter release, drawn from published data (Gleason et al. 1993; Martin and Ringham 1975) have been used to relate the size of the chloride conductance to its effect on transmitter release.

In contrast to the conclusion by Segev (1990), we find that even under the most favorable geometrical and electrical conditions for reducing transmitter release by a chloride conductance, the minimum steady-state conductance required is ~1 nS. This will be difficult to achieve, given the reported convergence of 1–3 axo-axonic synapses onto a single group Ia bouton (Maxwell et al. 1990), and the GABAergic quantal conductance of 150–300 pS (Kraszewski and Grantyn 1992; Ropert et al. 1990).

THE AXONAL MODEL

The axon

In the mammalian nervous system, axo-axonic contacts have been found only on the boutons of sensory nerves. One sensory nerve whose central projections have been studied in detail is the group Ia axon innervating primary stretch receptors in muscle spindles. The preterminal group Ia axon is myelinated to within 0.5–2.0 μm of the bouton. Axonal segments linking boutons are usually unmyelinated but are occasionally lightly myelinated. These unmyelinated axons have diameters in the range 0.1–0.4 μm, while the preterminal myelinated axons have diameters in the range 0.2–0.9 μm (Fyffe and Light 1984).

In this study both myelinated and unmyelinated nerve fibers are modeled, for comparison. The axons are 0.5 μm and 1 μm in diameter. The myelinated axon is surrounded by a myelin sheath 0.25 μm thick for the 1 μm axon, giving a total fiber diameter of 1.5 μm, and 0.125 μm thick for the 0.5 μm axon. Nodes of Ranvier are 2.5 μm wide and are spaced 60 μm apart (average values from Nicol 1988). A single bouton is sited in the middle of an axon and replaces a node of Ranvier in the myelinated axon. The axons are 1000 μm long, which is sufficient for the action potential in the bouton to be unaffected by any end effects.

The specific resistivity of the axoplasm (R_a) at 37°C is assumed to be 70 Ωcm, compared with 171 ± 23 Ωcm for rabbit nerve at 14°C (Chiu et al. 1979). As the Q_{10} for rabbit nerve was not stated, we referred to the measurements of Barrett and Crill (1974) and the discussion in Clements and Redman (1989) to obtain the value of 70 Ωcm. The specific membrane capacitance is assumed to be 1 μF/cm^2. The specific capacitance of the myelin is computed by assuming that the myelin consists of 100 layers of cell membrane per 1 μm of myelin thickness (Waxman and Wood 1984). This gives a myelin capacitance of 0.04 μF/cm^2 for the 1 μm axon. Resting membrane potential is assumed to be −80 mV.

Action potential propagation along an axon is computed by describing the axon as a series of connected, isopotential compartments. The membrane voltage in each compartment is calculated numerically using the backward Euler method of integration. Details of this method are given below.

The action potential

The conductance changes underlying the action potential in preterminal axons and nerve terminals are unknown. The action potential in these axons has been modeled on results obtained for peripheral myelinated nerve fibers in rabbit sciatic nerve (Chiu et al. 1979) scaled to a temperature of 37°C. The gross features of the action potential in unmyelinated nerve have been derived from extracellular recordings from 1 μm vagus nerve fibres (Paintal 1967). These characteristics are listed in Table 1. This table also shows the action-potential characteristics obtained by our models.

The action potential is generated by a sodium current for

the initial depolarizing phase, and a leak current for the repolarizing phase, with no voltage-dependent potassium current (Chiu et al. 1979). The sodium current is described by a Hodgkin-Huxley model with m^2h kinetics, where m and h are the activation and inactivation variables, respectively

$$I_{Na} = \bar{g}_{Na} m_2 h (V - E_{Na}) \quad (1)$$

$$\frac{dm}{dt} = (1 - m)\alpha_m(V) - m\beta_m(V) \quad (2)$$

$$\frac{dh}{dt} = (1 - h)\alpha_h(V) - m\beta_h(V) \quad (3)$$

At a temperature of 14°C

$$\alpha_m = \frac{0.029V + 10.1}{1 + \exp(-0.19V - 9.31)} \quad (4)$$

$$m_\infty = \frac{1}{1 + \exp(-0.24V - 13.44)} \quad (5)$$

$$\beta_m = \alpha_m\left(\frac{1}{m_\infty} - 1\right) \quad (6)$$

$$h_\infty = \frac{1}{1 + \exp(0.1775V + 13.26)} \quad (7)$$

$$\beta_h = \frac{1.25}{1 + \exp(-0.1V - 5.6)} \quad (8)$$

$$\alpha_h = \frac{h_\infty \beta_h}{1 - h_\infty} \quad (9)$$

The expressions for α_m and β_h were given explicitly by Chiu et al. (1979). The expressions for m_∞ and h_∞ were obtained by a best fit to the published data of Chiu et al. (1979). The equations are corrected for a temperature of 37°C by using a Q_{10} of 2.0 to scale the rate variables. The sodium reversal potential, E_{Na}, is 51 mV (Chiu et al. 1979).

The leak current is given by

$$I_{leak} = \bar{g}_{leak}(V - E_{leak}) \quad (10)$$

The average values for the sodium and leak conductances at the rabbit node of Ranvier are 2.2×10^{-4} mS and 0.31×10^{-4} mS, respectively (Chiu et al. 1979). The nodal area is, on average, 66 μm^2 (Ritchie and Rogart 1977). This gives a sodium conductance of 333 mS/cm^2 and a leak conductance of 47 mS/cm^2. These values formed the starting point for determining the parameters of the 1 μm myelinated axon. By trial and error, a nodal sodium conductance of 740 mS/cm^2, a nodal leak conductance of 47 mS/cm^2, and a Q_{10} of 2.0 were found to produce an action potential with the characteristics listed in Table 1. The leak conductance of the myelin was calculated by assuming the conductance of each layer of myelin was an order of magnitude less than at the node i.e., 4.7 mS/cm^2 (Waxman and Wood 1984). Given 25 layers of myelin (0.25 μm thickness of myelin), the myelin leak conductance was 0.188 mS/cm^2. There were assumed to be no sodium channels in the myelinated portion of the axon.

The density of sodium channels in unmyelinated membrane is one to two orders of magnitude less than that found in the node of Ranvier (Ritchie and Rogart 1977). Hence, sodium and leak conducances of 33.3 mS/cm^2 and 4.7 mS/cm^2, respectively, were taken as the starting point for finding the unmyelinated axon parameters. Again by trial and error, a sodium conductance of 105 mS/cm^2, a leak conductance of 4.7 mS/cm^2, and a Q_{10} of 2.0 were found to produce suitable action-potential characteristics for the 1 μm unmyelinated axon, as listed in Table 1.

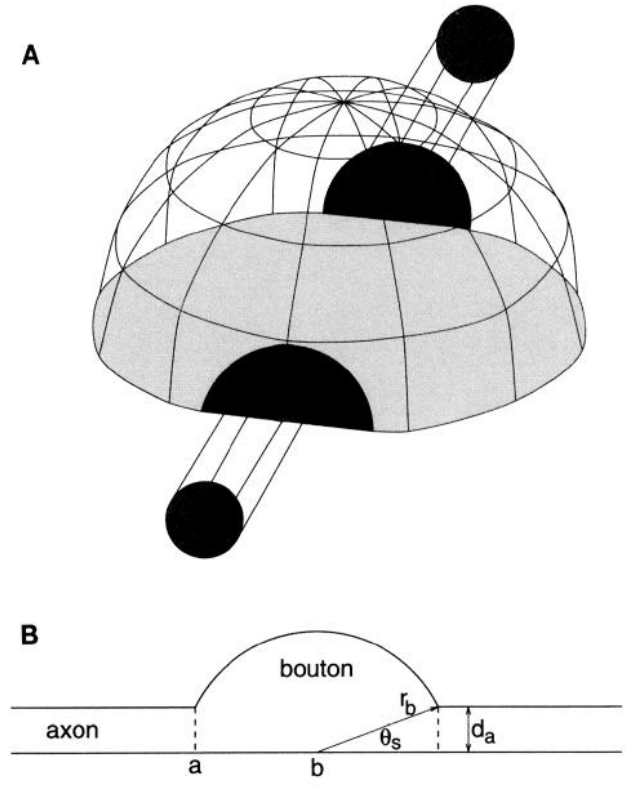

FIG. 1. A: hemispherical bouton; B: side view of bouton.

These same channel densities were used for the 0.5 μm axons, resulting in very similar action-potential characteristics but with reduced conduction velocities (unmyelinated: 0.8 m/s; myelinated: 2.5 m/s). The amplitude of the action potential in the myelinated nerve was slightly reduced (106 mV) because of the thinner covering of myelin.

The bouton

The large S-type boutons are roughly hemi-ellipsoidal in shape and have been reported by Maxwell et al. (1990) to be 1.2–4.1 μm along the major axis and by Fyffe and Light (1984) to 4–5 μm along the major axis. We have modeled the boutons as isopotential hemispheres, with diameters from 3–6 μm. Details of the bouton membrane properties are unknown. The hemispherical surface is modeled as a passive membrane (with only a leak conductance), or as an active membrane with the same properties as the connecting axon. The surface opposing the synaptic cleft is assumed to be passive. Presynaptic inhibition is modeled as a depolarizing chloride conductance, with a reversal potential of −40 mV (Deschenes et al. 1976). The geometry of the modeled bouton is shown in Fig. 1. The cylindrical axon attaches to a flat semicircular face on the side of the bouton adjacent to the base. The semicircular face has a radius equal to the diameter of the axon.

The expression for the axial resistance of a bouton is most easily obtained by considering a spherical bouton. The resis-

TABLE 2. *Axial resistance and active surface area for boutons of different diameter attached to axons of different diameter*

Bouton Diameter, μm	1 μm Axon		0.5 μm Axon	
	Resistance KΩ	Area, $\times 10^{-8}$ cm^2	Resistance KΩ	Area, $\times 10^{-8}$ cm^2
3	572	8	1047	11
4	587	17	920	21
5	559	29	817	34
6	524	44	736	51

tance of the hemispherical bouton is twice that of the spherical bouton. The resistance is given by integrating the equation for the axial resistance of a cylindrical segment over the length of the bouton with the cylindrical diameter being a function of the length. The derivation is as follows. Let

$x_1 = r_b - \sqrt{r_b^2 - d_a^2}$ and $x_2 = r_b$.

Then

$$\begin{aligned} R_b &= 4\int_{x_1}^{x_2} \frac{4R_a dx}{\pi d(x)^2} \\ &= \frac{16R_a}{\pi}\int_{x_1}^{x_2} \frac{dx}{(2\sqrt{2r_b x - x^2})^2} \\ &= \frac{4R_a}{\pi d_b}\left[\ln\left(\frac{x}{d_b - x}\right)\right]_{x_1}^{x_2} \\ &= \frac{4R_a}{\pi d_b}\ln\left(\frac{r_b + \sqrt{r_b^2 - d_a^2}}{r_b - \sqrt{r_b^2 - d_a^2}}\right) \end{aligned} \tag{11}$$

The active surface area of the bouton (i.e., where channels are present) is taken to be the hemispherical surface, not including the flat faces where the axon is attached, or the base. This area, A_b, is calculated as the area of the entire hemispherical surface minus the area of the surface that is missing due to the attachment of the axon

$$A_b = \frac{\pi d_b^2}{2} - 4r_b^2\theta_s \tag{12}$$

The angle, θ_s, is derived from the equation

$$\begin{aligned} (2d_a)^2 &= r_b^2 + r_b^2 - 2r_b r_b \cos 2\theta_s \\ \Rightarrow \theta_s &= \frac{1}{2}\arccos\left(1 - \frac{2d_a^2}{r_b^2}\right) \end{aligned} \tag{13}$$

Hence the active area of the bouton is given by

$$A_b = \frac{\pi d_b^2}{2} - 2r_b^2 \arccos\left(1 - \frac{2d_a^2}{r_b^2}\right) \tag{14}$$

The axial resistance and active surface area for boutons of different diameter attached to axons of different diameter are given in Table 2.

In this study a single bouton is sited in the middle of a long axon. The sodium and leak channel densities of the active bouton membrane are taken to either be the same as a node of Ranvier, or the same as unmyelinated membrane, depending on whether the axon is myelinated or unmyelinated. For a passive bouton, the sodium channel density is zero, and the leak channel density is the same regardless of the type of axon connected to the bouton. Its value is 4.7 mS/cm^2, which is the value used for the unmyelinated nerve.

COMPUTATIONAL METHODS

Compartmental model of an axon

Much work has been devoted to developing efficient and stable mathematical methods for solving compartmental models of axons based on the standard Hodgkin-Huxley kinetics (Cooley and Dodge 1966; Mascagni 1990, 1991; Moore and Ramon 1974; Parnas and Segev 1979; Parnas et al. 1976). We required a compartmental model in which the axial resistance and radius of each compartment could be different. The highly stable backward Euler method (Mascagni 1990) has been extended, as follows, to cater for this requirement.

The standard Hodgkin-Huxley type equation for the axon membrane potential is given by

$$C_m\frac{\partial V}{\partial t} = \frac{a}{2R_a}\frac{\partial^2 V}{\partial x^2} - \sum_{i=1}^{m} g_i(V - E_i) \tag{15}$$

where g_i is the conductance for ion i and E_i is the reversal potential for that conductance.

If the axon is described as a series of connected compartments, the membrane potential in a particular compartment, V_j, is given by the difference equation

$$C_j\frac{dV_j}{dt} = \frac{V_{j-1} - V_j}{(R_{j-1} + R_j)/2} - \frac{V_j - V_{j+1}}{(R_j + R_{j+1})/2} - \sum_{i=1}^{m_j} g_{i_j}(V_j - E_i) + I_{s_j} \tag{16}$$

where R_j is the axial resistance, C_j is the membrane capacitance and I_{s_j} is the injected current in the j^{th} compartment.

The series of equations describing the entire axon can be solved simultaneously using the backward Euler method of numerical integration. At each iteration the membrane potential of each compartment is calculated. This represents the value of the potential at a discrete point in time, $n\Delta t$, where n is the number of the iteration, and Δt is the discrete time step. At the $(n+1)^{st}$ iteration, the membrane potential of the j^{th} compartment is given by

$$\begin{aligned} C_j\frac{V_j^{n+1} - V_j^n}{\Delta t} &= \frac{V_{j-1}^{n+1} - V_j^{n+1}}{(R_{j-1} + R_j)/2} \\ &\quad - \frac{V_j^{n+1} - V_{j+1}^{n+1}}{(R_j + R_{j+1})/2} - \sum_{i=1}^{m_j} g_{i_j}^{n+1}(V_j^{n+1} - E_i) + I_{s_j}^{n+1} \end{aligned} \tag{17}$$

Collecting like terms the equation becomes

$$\begin{aligned} &-\frac{2\Delta t}{C_j(R_{j-1} + R_j)}V_{j-1}^{n+1} \\ &+\left(1 + \frac{2\Delta t}{C_j(R_{j-1} + R_j)} + \frac{2\Delta t}{C_j(R_j + R_{j+1})} + \frac{\Delta t}{C_j}\sum_{i=1}^{m_j} g_{i_j}^{n+1}\right)V_j^{n+1} \\ &-\frac{2\Delta t}{C_j(R_j + R_{j+1})}V_{j+1}^{n+1} = V_j^n + \frac{\Delta t}{C_j}\sum_{i=1}^{m_j} g_{i_j}^{n+1}E_i + \frac{\Delta t}{C_j}I_{s_j}^{n+1} \end{aligned} \tag{18}$$

If the axon consists of J compartments, we then have the tridiagonal system of equations

$$L_j V_{j-1}^{n+1} + D_j V_j^{n+1} + U_j V_{j+1}^{n+1} = B_j \quad j = 0, \ldots, J \tag{19}$$

where

$$L_j = -\frac{2\Delta t}{C_j(R_{j-1} + R_j)} \tag{20}$$

$$U_j = -\frac{2\Delta t}{C_j(R_j + R_{j+1})} \tag{21}$$

$$D_j = 1 - L_j - U_j + \frac{\Delta t}{C_j}\sum_{i=1}^{m_j} g_{i_j}^{n+1} \tag{22}$$

$$B_j = V_j^n + \frac{\Delta t}{C_j}\sum_{i=1}^{m_j} g_{i_j}^{n+1}E_i + \frac{\Delta t}{C_j}I_{s_j}^{n+1} \tag{23}$$

Taking symmetrical boundary conditions, such that $V_{-1} = V_1$ and $V_{J+1} = V_{J-1}$, gives

TABLE 3. *Compartmental parameters*

Compartment	Resistance	Capacitance	Total Current
Unmyelinated	$\frac{R_a \Delta x}{\pi a_j^2}$	$2\pi a_j \Delta x C_m$	$I_{Na} + I_{leak}$
Myelinated	$\frac{R_a \Delta x}{\pi a_j^2}$	$2\pi a_j \Delta x C_{myel}$	I_{myel_leak}
Node	$\frac{R_a \Delta x}{\pi a_j^2}$	$2\pi a_j (C_{myel}(\Delta x - N_L) + C_m N_L)$	$I_{Na}\frac{N_L}{\Delta x} + I_{node\_leak}\frac{N_L}{\Delta x} + I_{myel\_leak}\frac{(\Delta x - N_L)}{\Delta x}$
Bouton	$\frac{4R_a}{\pi d_b} \ln\left(\frac{r_b + \sqrt{r_b^2 - d_a^2}}{r_b - \sqrt{r_b^2 - d_a^2}}\right)$	$C_m\left(\frac{\pi d_b^2}{2} - 2r_b^2 \arccos\left(1 - \frac{2d_a^2}{r_b^2}\right)\right)$	$I_{Na} + I_{leak} + I_{Cl}$

C_{myel}, specific capacitance of the myelin; $I_{node\text{-}leak}$ and $I_{myel\text{-}leak}$ nodal leak current and the myelinated leak current, respectively; N_L, node length.

$$L_0 = 0 \tag{24}$$

$$L_J = -\frac{4\Delta t}{C_J(R_{J-1} + R_J)} \tag{25}$$

$$U_0 = -\frac{4\Delta t}{C_0(R_0 + R_1)} \tag{26}$$

$$U_J = 0 \tag{27}$$

Sodium channel dynamics

The conductances, g_{i_j}, for the leak and chloride channels are simply constants. However, the conductance of the sodium channel is a function of the membrane voltage. A discrete time approximation for the dynamics of the sodium channel activation variable, m, is given by

$$\frac{m_j^{n+1} - m_j^n}{\Delta t} = (1 - m_j^{n+1})\alpha_m(V_j^{n+1}) - m_j^{n+1}\beta_m(V_j^{n+1}) \tag{28}$$

$$\Rightarrow m_j^{n+1} = \frac{m_j^n + \alpha(V_j^{n+1})\Delta t}{1 + (\alpha_m(V_j^{n+1}) + \beta_m(V_j^{n+1}))\Delta t} \tag{29}$$

The equation for h is identical.

Integration scheme

The backward Euler method was implemented using a compartment size, Δx, of 10 μm, and a time step, Δt, of 10 μs.

Since the equations for the channel conductances, g_{i_j}, also depend on the membrane voltage, it is necessary to iterate the solving of the tridiagonal system of equations in series with the equations for the conductances, until the membrane voltages converge (Mascagni 1990). The following procedure is carried out at each time step.

Step 1: solve tridiagonal system using current values of channel conductances and membrane voltages,

Step 2: calculate new channel conductances using membrane voltages calculated in Step 1, and

Step 3: if the voltages have not converged (maximum change > 10^{-4}), repeat the procedure from Step 1.

Compartmental parameters

For the two models considered here, there are four different types of compartment: *1*) unmyelinated, *2*) myelinated, *3*) nodal, and *4*) bouton. A nodal compartment contains myelinated fiber on either side of the node of Ranvier. For a compartment length of 10 μm and a node length of 2.5 μm, there is 3.75 μm of myelinated fiber on each side of the node. The bouton replaces one of the nodal compartments in the myelinated axon.

The numerical integration scheme described above allows the axial resistance, capacitance and channel currents to be specified for each compartment, individually. These parameters are listed in Table 3 for each compartment type.

RESULTS

The propagation of the action potential along a 1 μm diameter unmyelinated axon containing an active bouton is shown in Fig. 2. The action potential is initiated by a brief current injection in the first compartment. The middle trace in each panel corresponds to the action potential in a 6 μm diameter bouton. The bottom panel shows the effect of

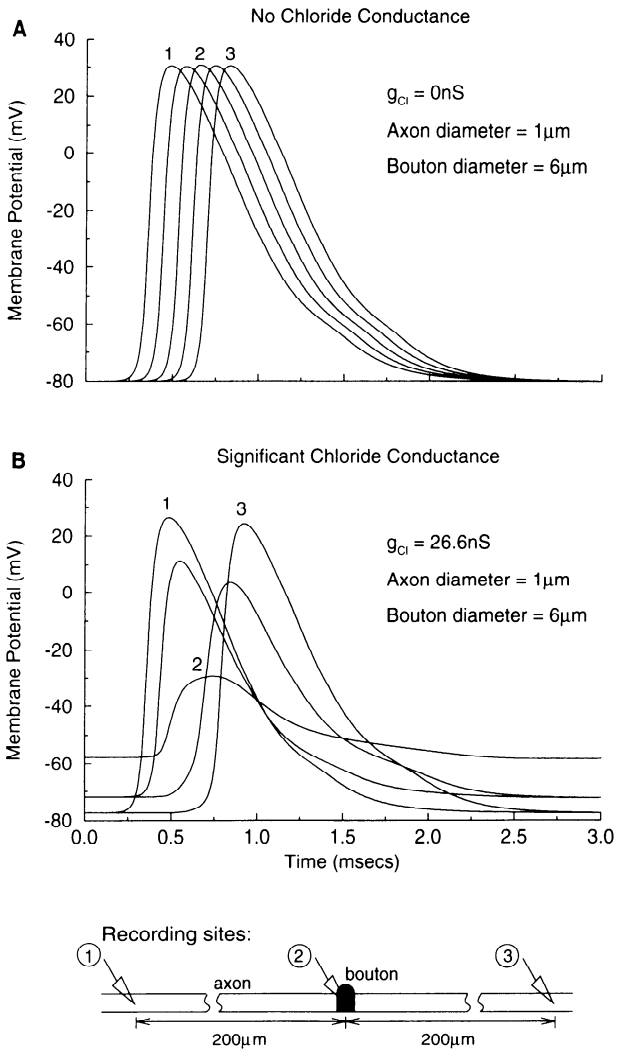

FIG. 2. Propagation of the action potential along an unmyelinated axon that contains an active bouton. Action potential recorded at 100 μm intervals, with the *middle trace* from the bouton. *A*: no chloride conductance; *B*: 26.6 nS chloride conductance in the bouton.

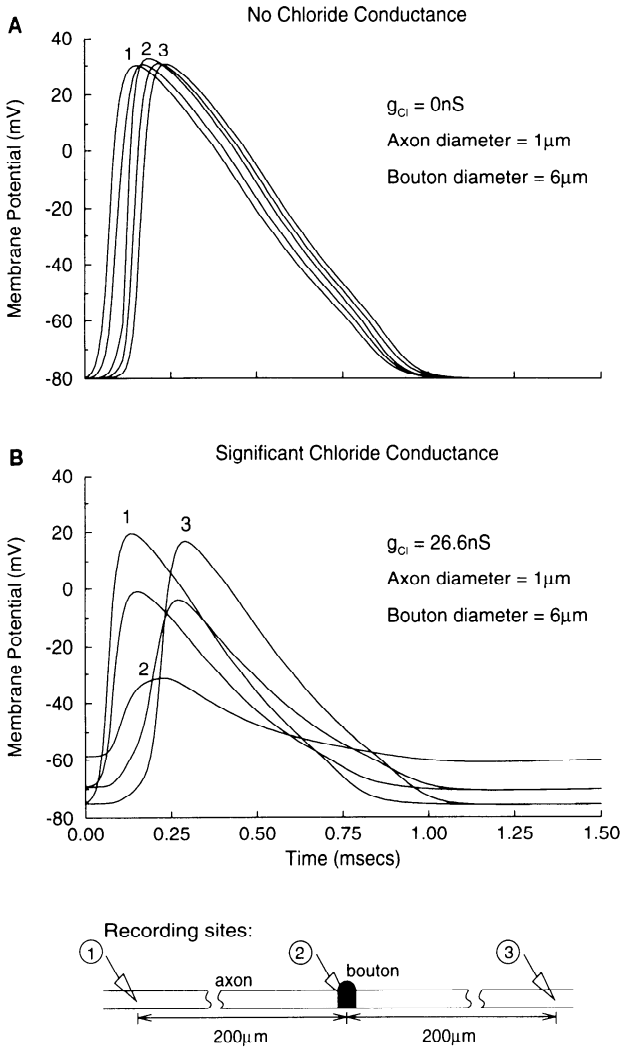

FIG. 3. Propagation of the action potential along a myelinated axon with an active bouton. Action potential recorded at 100 μm intervals, with the *middle trace* from the bouton. *A*: no chloride conductance; *B*: 26.6 nS chloride conductance in the bouton.

a chloride conductance in the bouton. The bouton and nearby axon are depolarized by the effects of the chloride conductance, with the depolarization in the bouton shown at time zero. While the action potential is severely attenuated in the bouton, it recovers quickly and continues to propagate along the axon. Similarly, the spread of an action potential along a 1 μm diameter myelinated axon containing a 6 μm diameter bouton is shown in Fig. 3. The bouton contains the same density of sodium and leak channels as the nodes. The action potential is almost identical in the bouton and in the axon when no shunt is present. A chloride shunt of 26.6 nS causes a 20 mV depolarization and a large decrease in the amplitude of the action potential in the bouton, but it recovers and continues to propagate.

Attenuation of the action potential by chloride conductance

The effect of different chloride conductances on the amplitude of the action potential in a 6 μm bouton with active membrane sited on a 1 μm axon is shown in Fig. 4. The same shunt causes a similar decrease in the amplitude of the action potential in both the myelinated and unmyelinated axons. Even with a significant decrease in the amplitude of the action potential in the bouton, the action potential continues to propagate through the bouton and along the distal axon. Propagation is finally blocked by a shunt of 43.9 nS that reduces the amplitude of the action potential to 36.3 mV in the bouton. For the unmyelinated axon, propagation is not blocked until a shunt of 64.7 nS is applied. This reduces the amplitude of the action potential in the bouton to 38.6 mV. The depolarization in the bouton caused by the chloride conductance is apparent at time zero in both panels of Fig. 4.

The calculations illustrated in Fig. 4 were repeated for 3, 4, and 5 μm diameter boutons attached to 1 and 0.5 μm diameter axons, myelinated and unmyelinated. The relationships between the amplitude of the action potential in the bouton and the chloride conductance for boutons and axons of different diameter are shown in Fig. 5. For an unmyelinated axon, the important parameters are *1*) chloride conductance and *2*) diameter of the axon. When the axon diameter is 1 μm, the action potential is unaltered in boutons ranging from 3 to 6 μm in diameter, for the same chloride conductance. If the bouton has a passive membrane there is a small increase in sensitivity to a chloride shunt with increasing bouton diameter due to an increase in the leak current. When the axon diameter is 0.5 μm, a chloride conductance also causes the same decrease in the action potential, regardless of bouton diameter (in the range 3–5 μm). A chloride conductance has a larger effect on the action potential in boutons attached to the smaller diameter axon. (Fig. 5*A*).

For myelinated nerve, the results for different bouton

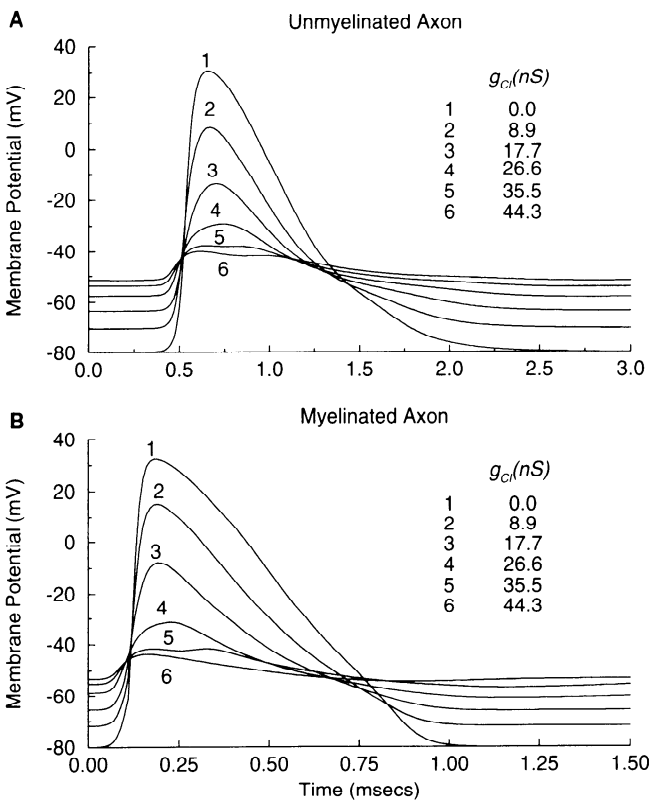

FIG. 4. Attenuation of the action potential amplitude in a bouton with an active membrane by different chloride conductances. The axon and bouton diameters are 1 and 6 μm, respectively. *A*: unmyelinated axon; *B*: myelinated axon.

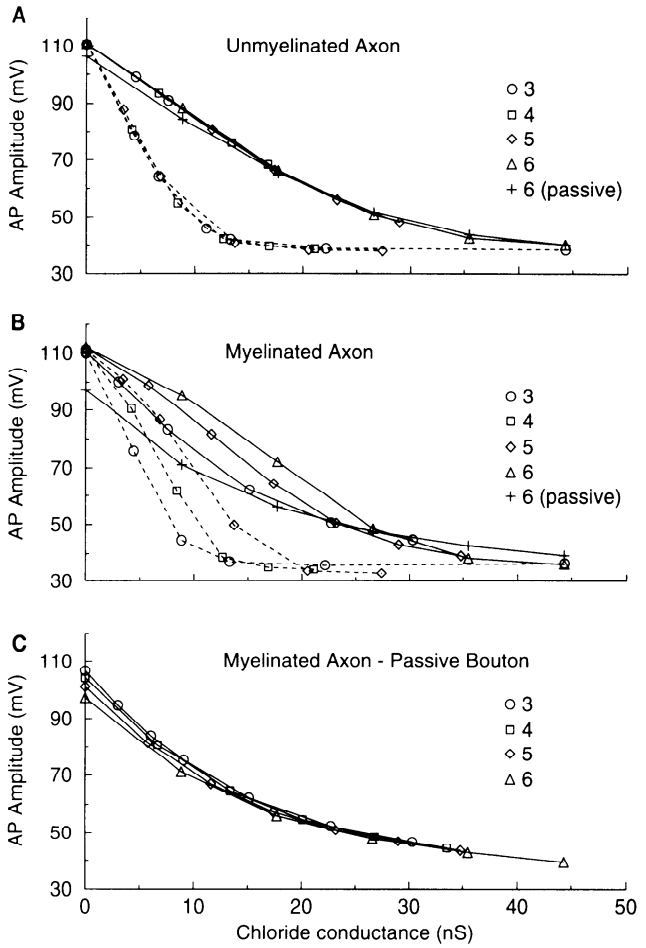

FIG. 5. Attenuation of the action potential amplitude as a function of chloride conductance for different diameter boutons and different diameter axons (*A*) unmyelinated axon, (*B*) myelinated axon, (*C*) myelinated axon with passive boutons. Solid lines are for 1 μm axons, broken lines are for 0.5 μm axons. Legends list bouton diameters in micrometers.

diameters cannot be grouped with axon diameter as they can for unmyelinated nerve. (Fig. 5*B*). The action potential is altered by different amounts for the same conductance on 3, 4, and 5 μm diameter boutons when each is attached to a 0.5 μm axon. Similarly, for a 1 μm diameter axon and bouton diameters from 3 to 6 μm, the same conductance alters the action potential by different amounts, with smaller diameter boutons being more sensitive to a given chloride conductance. When a bouton has a passive membrane, the action potential in the bouton is more attenuated than it is in a bouton with an active membrane, for identical geometry and chloride conductance.

The amount of depolarization of the bouton due to a chloride shunt is sensitive to bouton size when connected to a myelinated nerve but relatively insensitive to bouton size when attached to an unmyelinated nerve. For instance, for a 1 μm myelinated axon and a 15 nS conductance, the depolarization in boutons of diameter 3, 4, 5, and 6 μm is 19.3, 17.4, 14.9, and 12.6 mV, respectively. The corresponding values for a 1 μm unmyelinated axon attached to the same sized boutons are 15.3, 15.2, 15.0, and 14.8 mV. Here, the membrane properties of the unmyelinated axon are determining the depolarization in the bouton, while for the myelinated nerve, it is the leakage resistance associated with the surface area of the bouton relative to the conductance change that determines the depolarization. As the attenuation of the action potential is largely determined by depolarization induced inactivation of the sodium conductance in the bouton and the axon (discussed below), the action potential amplitude in boutons attached to myelinated nerve is sensitive to bouton size. The smaller the bouton size, the larger will be the depolarization for a given chloride shunt, and the larger will be the attenuation of the action potential (Fig. 5*B*).

When the bouton is passive, it presents an electrical load to an axon. Even when no conductance shunt is present, the action potential is attenuated in a bouton attached to a myelinated axon, because the bouton membrane becomes a current sink for the sodium conductances at adjacent nodes (Fig. 5*B*). With unmyelinated axons, this effect is largely swamped by the ability of the axon adjacent to the bouton to provide sufficient depolarizing current to the bouton membrane (Fig. 5*A*). This results in only a small decrease in the amplitude of the action potential relative to the amplitude in an active bouton.

In contrast with the results for active boutons attached to a myelinated axon, the action potential in passive boutons attached to a myelinated axon is largely independent of bouton diameter (Fig. 5*C*). Differences in action potential amplitude in different sized boutons are most obvious with no chloride conductance present. Under these circumstances, the electrical load created by the passive bouton on the sodium current from adjacent axon is smallest for the smallest boutons. The effects of sodium channel inactivation in the bouton membrane due to depolarization are no longer present.

Separating the effect of the conductance shunt from the effect of depolarization on the action potential

The depolarization caused by an increase in chloride conductance will partially inactivate the sodium channels, thereby reducing the amplitude of an action potential. Likewise, an action potential in a bouton will not develop its maximum amplitude if the membrane resistivity of nearby membrane is significantly reduced, even if the sodium channels are maximally activated. To separate the effects of sodium channel inactivation from the effects of a decrease in membrane resistivity, we calculated the action potential in boutons of various sizes when E_{Cl} equaled the resting potential (−80 mV) and when E_{Cl} equaled −40 mV, as shown in Fig. 6. The reduction in the action potential caused by depolarization is greater than the effect of the shunt acting alone. In the example illustrated in Fig. 6, the depolarization in the bouton attached to the myelinated nerve was within 2 mV of the depolarization in the bouton attached to the unmyelinated nerve over the entire range of conductances. The different slopes of the relationship between conductance and action potential amplitude for the two models when no depolarization is present is caused by the different leakage conductances used for the boutons attached to myelinated and unmyelinated axons.

Probability of transmitter release

The main reason for these simulations was to relate the magnitude of the chloride conductance to a reduction in transmitter release. The relationship between the probabil-

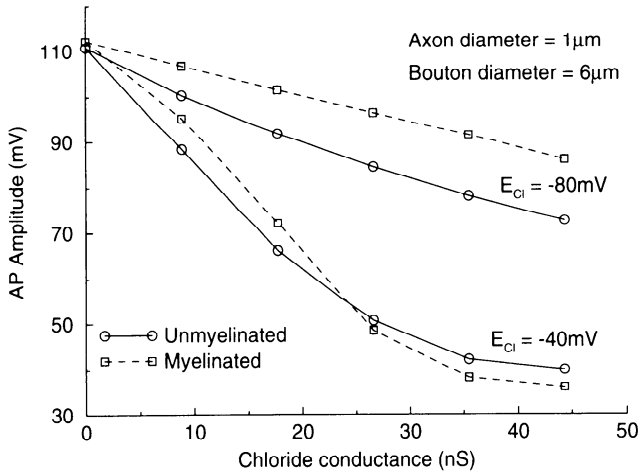

FIG. 6. Effect of chloride conductance on the amplitude of the action potential in a 6 μm active bouton sited on a 1 μm axon for both myelinated and unmyelinated axons. *Bottom lines*: a chloride reversal potential of −40 mV; and *top lines*: a chloride reversal potential of −80 mV (rest potential).

ity of transmitter release and the amplitude of the action potential in central nerve terminals is unknown. The closest result of this kind comes from combined recordings of the presynaptic action potential and postsynaptic potential for the synapse between a Müller axon and a lateral interneuron in the spinal cord of the lamprey (Martin and Ringham 1975). A simplified version of the relationship between pre- and postsynaptic potentials for the lamprey synapse is shown in Fig. 7*A*. If it is assumed that the probability of release is proportional to the amplitude of the EPSP, no decrease in transmitter release occurs until the action potential is smaller than 90 mV. If the amplitude of the action potential is replaced with the chloride conductance causing that amplitude, the result is shown in Fig. 7*B*. For a 1 μm unmyelinated axon and a 6 μm active bouton, transmitter release begins to decrease with a chloride conductance of 8 nS. The probability of release decreases in a slightly nonlinear way with increasing chloride conductance until it ceases at a conductance of 27 nS. The relationship for the 1 μm myelinated axon is similar but much more linear. Transmitter release is first affected by a conductance of 11 nS and ceases when the conductance is 26 nS. For the 0.5 μm diameter nerve and a 3 μm diameter bouton, release begins to be affected at 3 nS and is totally abolished at 8–9 nS. The conductances needed to reduce transmitter release in more elaborate geometries, such as axons terminating with a string of boutons, are discussed later.

Sensitivity of presynaptic inhibition to peak sodium conductance

All of the above results have been calculated for axons with particular densities of sodium and leakage channels. It is possible to obtain the required action potential characteristics for both the unmyelinated and myelinated axons with different combinations of peak sodium and leak conductances. To test the sensitivity of the results to the membrane conductances a number of alternative sets of parameters were found for each axon. This was done by choosing a new leak conductance and then altering the sodium conductance and the Q_{10} factor until the required action potential characteristics were found. Only the nodal conductances were altered in the myelinated axon. Figure 8 shows the chloride conductance required to attenuate the action potential to 50 mV (i.e., to block release) for different values

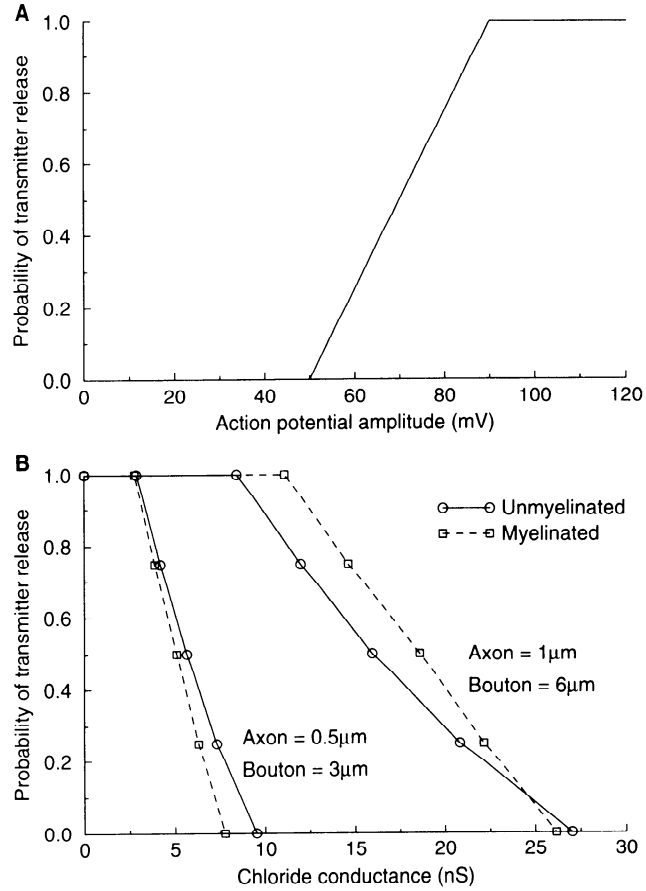

FIG. 7. *A*: a model of probability of transmitter release as a function of the amplitude of the action potential in a nerve terminal. *B*: probability of transmitter release in terms of the chloride conductance for active boutons of different diameters in unmyelinated and myelinated axons of different diameters.

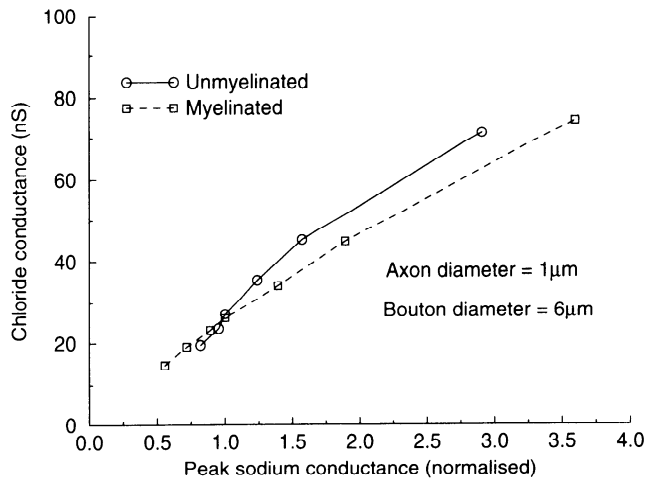

FIG. 8. Chloride conductance required to reduce action potential amplitude to 50 mV for axons with different peak sodium conductances. The peak sodium conductance is normalized to a conductance of 105 mS/cm^2 for the unmyelinated axon, and a nodal conductance of 740 mS/cm^2 for the myelinated axon.

of the sodium conductance. The peak sodium conductances have been normalized to their values in the standard axons used above. The greater the density of sodium channels, the larger the chloride conductance required to achieve the same attenuation of the action potential, as previously reported by Segev (1990).

DISCUSSION

The prevailing hypothesis on the mechanism of presynaptic inhibition is that activation of $GABA_A$ receptors increases a chloride conductance in the presynaptic membrane, thereby reducing the amplitude of the action potential and consequently, the calcium influx. An alternative, or at least additional mechanism, is that activation of $GABA_B$ receptors on axon terminals causes a reduction in transmitter release by reducing voltage-activated calcium currents via a second messenger (Dolphin and Scott 1987; Peng and Frank 1989a,b). This mechanism is not consistent with the recent demonstration that presynaptic inhibition of group Ia EPSPs was largely blocked by the $GABA_A$ antagonist, bicuculline, while the $GABA_B$ antagonist, saclofen, had little effect on presynaptic inhibition (Stuart and Redman 1992).

The calculations described in this paper for axon and bouton diameters similar to those observed for the terminal region of group Ia axons in the spinal cord, suggest that conductance increases in the synaptic bouton membrane in the range 3–10 nS are required to reduce transmitter release. Do conductances of this magnitude occur in the membrane of synaptic boutons? The quantal conductance for GABAergic synapses in the spinal cord is not known. It is 240–320 pS for CA1 pyramidal cells (Ropert et al. 1990); 200–400 pS in hippocampal granule cells (Edwards et al. 1990) and 105–135 pS in cultured tectal neurons (Kraszewski and Grantyn 1992). Using these values, it will require between 7 and 30 quanta to be released almost simultaneously at separate release sites on the same bouton if a conductance change of 3 nS is to be achieved. Furthermore, this conductance must be maintained by repetitive activity of interneurons. The number of P-type boutons on a Ia bouton has been reported to vary between one and three by Maxwell et al. (1990), with one being the most common observation. Some Ia boutons have no axo-axonic contacts. These small boutons appear to have no more than one active zone each. It does appear that for most Ia boutons, it will be difficult to achieve a conductance increase approaching 3 nS. Either the simulations have overestimated the conductance required to reduce transmitter release, or another mechanism in addition to the reduction of the action potential is required.

Model parameters

One of the main assumptions in the calculations concerns the active properties of the pre-terminal axons, and particularly the choice of sodium channel density. The sensitivity of the action potential to the chloride conductance depends on the sodium channel density (Segev 1990). A doubling of the channel density almost doubles the magnitude of the shunt required to alter the action potential, for both myelinated and unmyelinated nerves (Fig. 8). The peak sodium conductances used were 740 mS/cm^2 for the node and 105 mS/cm^2 for unmyelinated nerves. These values should be compared with ~1600 mS/cm^2 for the node in rat nerve and 290 mS/cm^2 for squid axon (both scaled to 37°C using a Q_{10} of 1.3) (Hille 1992, Table 3). The peak sodium conductances used in the simulations were chosen to give the observed time course and conduction velocity for the action potential in both types of axon. As the values used are smaller than those obtained from the literature, their choice may exaggerate the effects of conductance changes.

No potassium channels were included in the axonal membrane or in the membrane of active boutons. The membrane currents that were used were derived from measurements of nodal currents in mammalian axons (Chiu et al. 1979). Potassium currents exist in the terminals of posterior pituitary axons (Bielefeldt et al. 1992). Transmitter release at central synapses is increased by 4-aminopyridine (4-AP) (Jack et al. 1981; Jankowska et al. 1977) and one interpretation of this result is that 4-AP prolongs the duration of the action potential in nerve terminals by blocking potassium channels. Additional calculations were made to assess the importance of including potassium channels in active membrane. A delayed potassium current with the kinetics and activation characteristics described by Chiu and Ritchie (1980) for the internode was used, with $\bar{g}_K$ = 10 mS/cm^2, $\bar{g}_{leak}$ = 5.4 mS/cm^2 and Q_{10} = 1.7. In a 1 μm unmyelinated nerve and a 6 μm active bouton, the conductance required to reduce the action potential to 90 mV (threshold for presynaptic inhibition) was 9.3 nS when potassium channels were present in the nerve and bouton, compared with 8.4 nS when they were absent. A larger conductance is required to reduce the action potential, because the depolarization caused by the chloride conductance partially activates the potassium conductance. The net depolarization is smaller than it would be if no potassium channels were present. This causes less inactivation of the sodium current. The effect of including a potassium conductance in the bouton and unmyelinated axon was small and made the action potential more resistant to the effects of a chloride conductance.

Another assumption is the leakage conductance of the bouton membrane. It seemed reasonable to make this the same as the leakage conductance of nodal membrane for an active bouton attached to a myelinated nerve (47 mS/cm^2) and the same as the leakage conductance of unmyelinated membrane for an active bouton attached to an unmyelinated nerve (4.7 mS/cm^2). This same leak conductance was maintained in the unmyelinated model when the bouton was converted to passive membrane. However, if the leak conductance appropriate for nodal membrane was used for a passive bouton attached to myelinated nerve, the consequences were dramatic. Without additional shunt conductances, the action potential was greatly attenuated for some geometries. For instance, the amplitude of the action potential in a 6 μm passive bouton attached to a 1 μm myelinated axon, was 57 mV. This is not surprising because the leak conductance in such a bouton was 21 nS. Because our objective was to examine the sensitivity of the action potential to chloride conductances, it seemed inappropriate to use such a leak conductance, so we used the same value (4.7 mS/cm^2) as was used for passive boutons attached to unmyelinated nerve.

The relationship between amplitude of the presynaptic action potential and the postsynaptic potential has been derived from two different synapses. One is a synaptic contact between amacrine cells in culture (Gleason et al. 1993). These synapses are activated by graded potentials rather than action potentials. Transmitter release begins when the presynaptic cell is depolarized to −40 mV and continuously increases for more depolarized potentials. The other synaptic system (which operates with action potentials) is in the lamprey spinal cord, between a Müller axon and a lateral interneuron (Martin and Ringham 1975). Threshold depolarization for transmitter release is 40 to 50 mV from rest, with saturation occuring at ~100 mV depolarization from rest. It is an assumption that the results of these two synaptic systems can be transferred to group Ia synapses.

During presynaptic inhibition of single group Ia fiber EPSPs in motoneurons, where several release sites are usually involved in transmission at the Ia synapse, the probability of release at some release sites is not affected while at others it is reduced (Clements et al. 1987). Some boutons may not receive axo-axonic synapses. Others that have axo-axonic contacts may have their release probabilities reduced by different amounts. The result is that presynaptic inhibition, when averaged across the various release sites at which an EPSP is generated, is a graded process. The appropriate interpretation of Fig. 7, *A* and *B* is that they represent averages across many release sites.

Integrative implications of the effect of chloride shunts on axon terminals

To achieve simulated presynaptic inhibition with a conductance of 3 nS, it has been necessary to choose some variables at the margins of their likely range. For instance, bouton to axon diameter ratios of 6:1 to 10:1 were used. Several P-type boutons must converge onto a synaptic terminal. The peak sodium conductances used are lower than those reported for peripheral axons, and potassium currents have not been included.

Another way of making the action potential more sensitive to a conductance increase is to string together synaptic boutons sufficiently close so they are not electrically isolated from each other and to apply conductance changes to each bouton simultaneously. This type of scheme has recently been investigated by Segev (1990). The termination patterns of group Ia afferents usually have several boutons en passant, followed by a terminating bouton (Brown and Fyffe 1981). These boutons are separated by 10–20 μm, and the linking axons are unmyelinated with diameters 0.1 to 0.4 μm (Fyffe and Light 1984). The diagram attached to Table 4 illustrates two schemes of this kind, where three boutons are each separated by 10 μm. They can have active or passive membrane. Conductance increases were applied to all three boutons, and the action potential was monitored in either the terminal bouton (for the terminating arrangement) or the central bouton (for the en passant scheme). The monitoring locations are the most sensitive to the chloride shunt in both examples. Table 4 lists the chloride conductances needed to reduce the action potential to 90 mV, i.e., the putative threshold for presynaptic inhibition. If the results for a 0.5 μm axon and 3 μm bouton are followed, a single en passant active bouton requires 3 nS (Fig. 7*B*), three en passant active boutons must each receive 1.1 nS, and three en passant passive boutons each need 0.7 nS. When the axon terminates at the third bouton, each active bouton must receive 0.9 nS, and 0.6 nS for each passive bouton. Smaller conductances are required when the coupling axons have diameters of 0.1 and 0.2 μm. When the axon terminates in a bouton, the input resistance at the terminating bouton is higher than when the bouton is en passant. This causes the depolarization arising from the chloride conductance to be greater in a terminating structure than in an en passant arrangement. Thus terminating structures provide a greater effect on the action potential for a particular conductance, because of the greater inactivation of the sodium conductance. The conductances required to depress the action potential to 90 mV in these multiple bouton arrangements are approaching the peak quantal conductances for GABA. However, it should be emphasized that larger conductances will be required to achieve significant presynaptic inhibition.

TABLE 4. *Chloride conduction required to reduce the action potential amplitude to 90 mV for different configurations of multiple boutons on unmyelinated axons*

Bouton Position	Bouton Membrane	Axon Diam, μm	Bouton Diam, μm	Chloride Shunt, nS
En passant	Active	1	6	3.2
En passant	Active	0.5	3	1.1
En passant	Active	0.2	1.2	0.3
En passant	Active	0.2	3	0.4
En passant	Active	0.1	0.6	0.1
En passant	Active	0.1	3	0.2
En passant	Passive	1	6	1.6
En passant	Passive	0.5	3	0.7
En passant	Passive	0.2	1.2	0.2
Terminal	Active	1	6	2.7
Terminal	Active	0.5	3	0.9
Terminal	Passive	1	6	1.2
Terminal	Passive	0.5	3	0.6

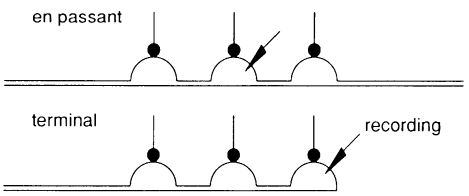

Complete abolition of release could occur without extinguishing the action potential. While action potentials smaller than 50 mV peak were assumed to cause no release, action potentials were not blocked by the conductance shunt until their amplitude was less than 40 mV. This required shunts of 44 and 65 nS for a 1 μm axon–6 μm active bouton system (myelinated and unmyelinated, respectively). For the 0.5 μm axon–3 μm bouton, the corresponding shunts are 10 and 16 nS. These conductances are approximately twice as large as the conductances required to completely abolish release. If presynaptic inhibition is to act independently at different boutons associated with the same preterminal axon, it is important that the conductance shunts which block impulses at boutons en passant are clearly greater than the range of shunts which only alter release probabilities.

The simulations reported in this paper are an extension of a recent analysis by Segev (1990). Segev's analysis showed that a conductance of 20 to 40 nS placed at the termination of a 1 μm axon reduced the action potential at the termination to 20 mV or less, i.e., less than that required for transmitter release. Smaller conductances (10 nS) were required to reduce the action potential to 10 mV in a string of two varicosities linked by 0.1 μm axons. The results in this paper for large axons and large bouton sizes are largely in agreement with Segev's results, even though we have used both myelinated and unmyelinated axons with membrane characteristics obtained from mammalian nerve and scaled the kinetics of the membrane currents to 37°C.

However, by including a chloride equilibrium potential of −40 mV, we have shown that the dominant effect of a chloride conductance on the action potential arises from inactivation of the sodium channels. This effect becomes more prominant as the dimensions of the boutons and axons become smaller and the input resistance at the boutons consequently increases. Inclusion of presynaptic depolarization led to simulations that indicate presynaptic inhibition could be achieved with much smaller conductances than those calculated by Segev (1990). The direct effect of GABA on sodium channel inactivation has recently been demonstrated at secretary nerve endings (Zhang and Jackson 1993).

By focusing on the conductance changes that are required to reduce transmitter release, and by considering axonal termination schemes in which several large boutons are linked by fine axons, conditions for reducing transmitter release with a conductance of ~1 nS have been achieved. However, as synaptic boutons (in the spinal cord) receive from zero to three axo-axonic contacts (Maxwell et al. 1990), and as the peak quantal conductance for GABA has been measured in the range 150–300 pS (Kraszewski and Grantyn 1992; Ropert et al. 1990), we suggest that achieving a maintained conductance of 1 nS at each of several adjacent boutons will be difficult.

An additional mechanism by which calcium influx could be modulated is by inactivation of voltage-dependent calcium channels. Depolarizations in nerve terminals of 10–20 mV were observed in the simulations reported in this paper, and similar depolarizations were measured in secretary nerve terminals by Zhang and Jackson (1993). Depolarizations of this magnitude from the resting potential would partially inactivate the high threshold calcium channels that have been shown to be present in dorsal root ganglion cells (Fox et al. 1987) and are thought to be present in nerve terminals.

Preliminary work on the equations for the channel activation and inactivation curves was done by J. Cassell. An example of software for solving tridiagonal systems of equations was kindly provided by Dr. Michael Mascagni. Drs. Bruce Walmsley and Rosemary Martin made useful suggestions on improving the manuscript. We are grateful for their contributions.

Address for reprint requests: S. J. Redman, Div. of Neuroscience, JCSMR, P.O. Box 334, Canberra, A.C.T., 2601, Australia.

Received 10 June 1993; accepted in final form 25 August 1993.

REFERENCES

BARRETT, J. N. AND CRILL, W. E. Specific membrane properties of cat motoneurones. *J. Physiol. Lond.* 239: 301–324, 1974.

BIELEFELDT, K., ROTTER, J. L., AND JACKSON, M. B. Three potassium channels in rat posterior pituitary nerve terminals. *J. Physiol. Lond.* 458: 41–67, 1992.

BROWN, A. G. AND FYFFE, R. E. W. Direct observations on the contacts made between Ia afferent fibres and gamma-motoneurones in the cat's lumbosacral spinal cord. *J. Physiol. Lond.* 313: 121–140, 1981.

BURKE, R. E. AND RUDOMIN, P. Spinal neurones and synapses. In: *Handbook of Physiology. The Nervous System. Cellular Biology of the Neurons.* Bethesda, MD: Am. Physiol. Soc., 1977, sect. 1, vol. I, p. 877–944.

CHIU, S. Y. AND RITCHIE, J. M. Potassium channels in nodal and internodal axonal membrane of mammalian myelinated fibres. *Nature Lond.* 284: 170–171, 1980.

CHIU, S. Y., RITCHIE, J. M., ROGART, R. B., AND STAGG, D. A quantitative description of membrane currents in rabbit myelinated nerve. *J. Physiol. Lond.* 292: 149–166, 1979.

CLEMENTS, J. D., FORSYTHE, I. D., AND REDMAN, S. J. Presynaptic inhibition of synaptic potentials evoked in cat spinal motoneurones by impulses in single group Ia axons. *J. Physiol. Lond.* 383: 153–169, 1987.

CLEMENTS, J. D. AND REDMAN, S. J. Cable properties of cat spinal motoneurons measured by combining voltage clamp, current clamp and intracellular staining. *J. Physiol. Lond.* 409: 63–87, 1989.

CONRADI, S., CULLHEIM, S., GOLLVIK, L., AND KELLERTH, J.-O. Electron microscopic observations on the synaptic contacts of Group Ia muscle spindle afferents in the cat lumbrosacral cord. *Brain Res.* 265: 31–39, 1983.

COOLEY, J. W. AND DODGE, F. A. Digital computer solutions for excitation and propagation of the nerve impulse. *Biophys. J.* 6: 583–599, 1966.

DESCHENES, M., FELTZ, P., AND LAMOUR, Y. A model for an estimate *in vivo* of the ionic basis of presynaptic inhibition: an intracellular analysis of the GABA-induced depolarization of rat dorsal root ganglion. *Brain Res.* 118: 486–493, 1976.

DOLPHIN, A. C. AND SCOTT, R. H. Calcium channel currents and their inhibition by (−)baclofen in rat sensory neurones: modulation by guanine nucleotides. *J. Physiol. Lond.* 386: 1–17, 1987.

EDWARDS, F. A., KONNERTH, A., AND SAKMANN, B. Quantal analysis of inhibitory synaptic transmission in the dentate gyrus of rat hippocampal slices: a patch-clamp study. *J. Physiol. Lond.* 430: 213–249, 1990.

FOX, A. P., NOWYCKY, M. C., AND TSIEN, R. W. Kinetic and pharmacological properties distinguishing three types of calcium currents in chick sensory neurones. *J. Physiol. Lond.* 394: 149–172, 1987.

FRANK, K. AND FUORTES, M. G. F. Presynaptic and postsynaptic inhibition of monosynaptic reflexes. *Fed. Proc.* 16: 39–40, 1957.

FYFFE, R. E. W. AND LIGHT, A. R. The ultrastructure of Group Ia afferent fiber synapses in the lumbrosacral spinal cord of the cat. *Brain Res.* 300: 201–209, 1984.

GLEASON, E., BORGES, S., AND WILSON, M. Synaptic transmission between pairs of retinal amacrine cells in culture. *J. Neurosci.* In press.

HILLE, B. *Ionic Channels of Excitable Membranes.* Sunderland, MA: Sinauer, 1992.

JACK, J. J. B., REDMAN, S. J., AND WONG, K. Modifications to synaptic transmission at group Ia synapses on cat spinal motoneurones by 4-aminopyridine. *J. Physiol. Lond.* 321: 111–126, 1981.

JANKOWSKA, E., LUNDBERG, A., RUDOMIN, P., AND SYKOVA, E. Effects of 4-aminopyridine on transmission at excitatory and inhibitory synapses in the spinal cord. *Brain Res.* 136: 387–392, 1977.

KRASZEWSKI, K. AND GRANTYN, R. Unitary, quantal and miniature GABA-activated synaptic chloride currents in cultured neurons from the rat superior colliculus. *Neuroscience* 47: 555–570, 1992.

MARTIN, A. R. Junctional transmission II. Presynaptic mechanisms. In: *Handbook of Physiology. The Nervous System. Cellular Biology of the Neurons.* Am. Physiol. Soc., 1977, sect. 1, vol. I, p. 329–356.

MARTIN, A. R. AND RINGHAM, G. L. Synaptic transfer at a vertebrate central nervous synapse. *J. Physiol. Lond.* 251: 409–426, 1975.

MASCAGNI, M. The backward Euler method for numerical solution of the Hodgkin-Huxley equations of nerve conduction. *SIAM J. Numer. Anal.* 27: 941–962, 1990.

MASCAGNI, M. A parallelizing algorithm for computing solutions to arbitrarily branched cable neuron models. *J. Neurosci. Methods* 36: 105–114, 1991.

MAXWELL, D. J., CHRISTIE, W. M., SHORT, A. D., AND BROWN, A. G. Direct observations of synapses between GABA-immunoreactive boutons and muscle afferent terminals in lamina VI of the cat's spinal cord. *Brain Res.* 530: 215–222, 1990.

MOORE, J. W. AND RAMON, F. On numerical integration of the Hodgkin and Huxley equations for a membrane action potential. *J. Theor. Biol.* 45: 249–273, 1974.

NICOL, M. J. *A Light and EM Study of Clarke's Column.* (PhD Thesis). Canberra, A.C.T., Australia: The Australian National University, 1988.

NICOLL, R. A. AND ALGER, B. E. Presynaptic inhibition: transmitter and ionic mechanisms. *Int. Rev. Neurobiol.* 21: 217–258, 1979.

PAINTAL, A. S. A comparison of the nerve impulses of mammalian non-medullated nerve fibres with those of the smallest diameter medullated fibres. *J. Physiol. Lond.* 193: 523–533, 1967.

PARNAS, I., HOCHSTEIN, S., AND PARNAS, H. Theoretical analysis of parameters leading to frequency modulation along an inhomogeneous axon. *J. Neurophysiol.* 39: 909–923, 1976.

PARNAS, I. AND SEGEV, I. A mathematical model for conduction of action potentials along bifurcating axons. *J. Physiol. Lond.* 295: 323–343, 1979.

PENG, Y. AND FRANK, E. Action of $GABA_B$ receptors causes presynaptic inhibition at synapses between muscle spindle afferents and motoneurons in the spinal cord of bullfrogs. *J. Neurosci.* 9: 1502–1515, 1989a.

PENG, Y. AND FRANK, E. Activation of $GABA_B$ receptors causes presynaptic and postsynaptic inhibition at synapses between muscle spindle and motoneuron in the spinal cord of bullfrogs. *J. Neurosci.* 9: 1516–1522, 1989b.

RITCHIE, J. M. AND ROGART, R. B. Density of sodium channels in mammalian myelinated nerve fibres and nature of the axonal membrane under the myelin sheath. *Proc. Natl. Acad. Sci. USA* 74: 211–215, 1977.

ROPERT, N., MILES, R., AND KORN, H. Characteristics of miniature inhibitory post-synaptic currents in CA1 pyramidal neurones of rat hippocampus. *J. Physiol. Lond.* 428: 707–722, 1990.

SEGEV, I. Computer study of presynaptic inhibition controlling the spread of action potentials into axonal terminals. *J. Neurophysiol.* 63: 987–998, 1990.

STUART, G. J. AND REDMAN, S. J. The role of $GABA_A$ and $GABA_B$ receptors in presynaptic inhibition of Ia EPSPs in cat spinal motoneurones. *J. Physiol. Lond.* 447: 675–692, 1992.

WATSON, A. H. D. Presynaptic modulation of sensory afferents in the invertebrate and vertebrate nervous system. *Comp. Biochem. Physiol.* 103: 227–239, 1992.

WAXMAN, S. G. AND WOOD, S. L. Impulse conduction in inhomogeneous axons: effects of variation in voltage-sensitive ionic conductances on invasion of demyelinated axon segments and preterminal fibers. *Brain Res.* 294: 111–122, 1984.

ZHANG, S. J. AND JACKSON, M. B. GABA activated chloride channels in secretory nerve endings. *Science Wash. DC* 259: 531–534, 1993.